Pure & Appl. Chem., Vol. 52, pp.93-118.
Pergamon Press Ltd. 1979. Printed in Great Britain.

0033-4545/80/0101-0093 $02.00/0

ELECTRONIC STRUCTURE OF TRANSITION METAL COMPOUNDS; GROUND-STATE PROPERTIES OF THE 3d-MONOXIDES IN THE ATOMIC SPHERE APPROXIMATION

O.K. Andersen, H.L. Skriver, H. Nohl,
Max-Planck-Institut für Festkörperforschung, 7 Stuttgart 80, FRG

B. Johansson
Department of Physics, Sect. 214, FOA2, S-10450, Sweden

Abstract - We give an introduction to the so-called atomic sphere approximation (ASA) for describing and computing band structures and ground-state properties of closely packed crystals. The concepts of canonical bands, potential parameters and partial pressures are explained. As an example we discuss the band structures of the 3d-monoxides which exhibit ionic insulating- (CaO), metallic- (TiO and VO) and antiferromagnetic insulating (MnO) behaviour. The band structures have been calculated self-consistently as functions of the lattice constants and para-, ferro-, and antiferromagnetic spin-polarizations have been allowed for within the local approximation to the spin-density functional formalism. We find good agreement between the calculated and observed equilibrium lattice constants even for the antiferromagnetic Mott insulators (MnO through NiO), despite our incorrect description of their ground state.

INTRODUCTION

The numerous band-structure calculations performed during the last two decades show that the electronic structure of crystals, metals in particular, is described rather well in a one-electron picture where the effects of exchange and correlation are treated in a statistical way, as in the Slater exchange-, Xα-, or density-functional schemes (1-3). With the advent of larger computers, improved programming and new, effective band-structure methods it has, in the last decade, become possible to carry through such calculations to self-consistency and hence, to obtain parameter-free estimates of ground-state properties such as cohesive energies, lattice constants, compressibilities, magnetic moments, a.s.o. So far, calculations of ground-state properties using the density-functional scheme (2,3) have been carried out successfully for nearly all elemental metals (4-9), for a number of diatomic molecules (10) and, most recently, for a few compounds with the simple CsCl- and NaCl-structures (11,12). The latter calculation,performed for the series of 3d-monoxides,is the subject of the present paper.

Many of the above mentioned calculations (6-12) have been performed with some form of the linear muffin-tin orbitals (LMTO) method (13,14) which is computationally very fast and conceptually simple. The method may be employed at various levels of sophistication; the most accurate, and cumbersome, is the one used in the calculations (10) for diatomic molecules with their highly aspherical charge distributions. A level of great conceptual simplicity is the so-called atomic sphere approximation (ASA) (14-17) where space is divided into overlapping atomic spheres inside which the electronic charge is assumed to be spherically symmetric. This approximation is best for closely packed materials without directional bonds and it has, for instance, been used successfully for elemental metals (6-9, 18), intermetallic compounds (19), A-15 materials (20), Laves phases (21), Chevrel phases (22,23), ternary Rh-Borides (24), and U-pnictides (26).

In the present paper we shall explain some simple aspects of the ASA and discuss how it can be used to calculate equilibrium lattice constants, compressibilities and magnetic moments. As an example we consider the series of 3d-monoxides, CaO through NiO, together with CaS.

The monoxides of the 3d-elements all crystallize in the rocksalt structure but, otherwise, they have very different physical properties (26): CaO is a diamagnetic, ionic insulator, TiO and VO are paramagnetic metals, TiO is even a superconductor, and MnO through NiO are antiferromagnetic Mott insulators (27). Therefore, as we proceed through the series, a Mott metal-insulator transition takes place before reaching MnO. This view that there is a fundamental difference between the lighter and the heavier monoxides has found further support from the behaviour of the lattice constants which, as shown in Fig. 1, are substantially contracted for the metallic compounds as compared with the insulating ones (28). In addition, the binding energy is considerably enhanced for the metallic compounds (29). Apparently, when metallic, the 3d-electrons give rise to an additional cohesion beyond the ionic binding for the insulating monoxides.

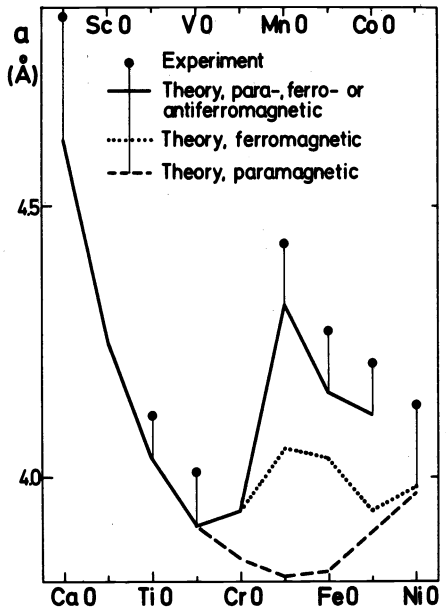

Fig. 1. Experimental and theoretical lattice constants for the 3d-monoxides.

It is well known that the usual band picture cannot properly describe the ground state of a Mott insulator and, hence, the electronic structure of MnO through NiO. For these systems we will, however, focus our attention on the experimental fact that they are all antiferromagnetic (30) and, in our self-consistent band calculations, we will therefore allow for ferro- and antiferromagnetic spin-polarization. With this approach we do correctly find that, for MnO through NiO, antiferromagnetic solutions with completely separated d-subbands are stable and that, with these solutions, the lattice constants are well reproduced. This is shown in Fig. 1. Nevertheless, as anticipated (30), the antiferromagnetic band structures incorrectly yield Fermi surfaces for all the Mott insulators except MnO where the d-band is half full.

There exists a vast literature on the electronic structure of the 3d-monoxides and references may be found in the review by Adler (26) and the more recent article by Brandow (30). As regards previous band-structure calculations we shall mention three. Ten years ago Wilson (31) performed a non-self-consistent, antiferromagnetically spin-polarized calculation for MnO at the observed lattice constant and he found that the Mn d-subbands were completely separated. In 1971 Mattheiss (32) performed non-self-consistent calculations for the entire series without allowing for spin-polarization and using Slater exchange. For the antiferromagnetic insulators he constructed Wannier functions from his bands and extracted crystal-field parameters. By comparing these with experimental values he concluded that his d-bands were about 30 per cent too narrow, i.e. that they should be about 0.3 Ry wide. From the calculated d-bandwidths Heine (28) estimated the size of the d-electron contribution to the binding and, using the experimental value for the compressibility, he concluded that this was roughly consistent with the hump observed in the lattice constant when the d-electrons undergo the Mott localization (Fig. 1). In 1976 Neckel and coworkers (33) presented self-consistent, Xα-energy bands for the lighter monoxides ScO, TiO and VO at the observed lattice constants. These bands were about 30 per cent wider than those of Mattheiss, and Schwarz et al. (34) used them to calculate K- and L-edge emission and absorption spectra which they found were in good agreement with the experimental results.

Our self-consistent energy bands for the lighter monoxides are rather similar to those of Neckel et al. We use the Hedin-Lundquist and Barth-Hedin (3) forms of the exchange-correlation potential and we perform the calculations for a range of lattice constants. The variation in the total energy is evaluated and the equilibrium lattice constants determined.

ATOMIC SPHERE APPROXIMATION AND BAND STRUCTURES OF THE 3d-MONOXIDES

We shall now give an introduction to the ASA(14-17) in which we concentrate on the conceptually most simple aspects and leave out technical details.

Let us first suppose that we want to solve Schrödingers equation for one electron moving in a

potential having the so-called muffin-tin form indicated in Fig. 2. This form is spherically symmetric inside non-overlapping muffin-tin spheres surrounding the atoms and flat in between. For any prescribed energy, E, one can always solve Schrödingers differential equation for one isolated muffin-tin sphere embedded in the flat potential, V_{mtz}, by numerically integrating the radial Schrödinger equation outwards from the sphere centre and, at the sphere boundary, attach continuously and differentiably a linear combination of the free-space spherical Bessel- and Neumann functions with the appropriate wavenumber $\kappa = (E-V_{mtz})^{1/2}$. This solution is a phase-shifted spherical-, or partial, wave. For the crystalline muffin-tin potential one may now centre a linear combination of such partial waves on each atomic site, $\vec{R}$, in the crystal and ask whether one can determine the linear combination in such a way that it constitutes a solution of Schrödingers equation for the entire crystal. The condition must be that, inside any sphere, the sum of the partial-wave tails coming from all the other spheres must interfere destructively. If formulated mathematically this gives rise to the so-called KKR-(35)or scattered-wave (36) method which is fairly complicated to handle.

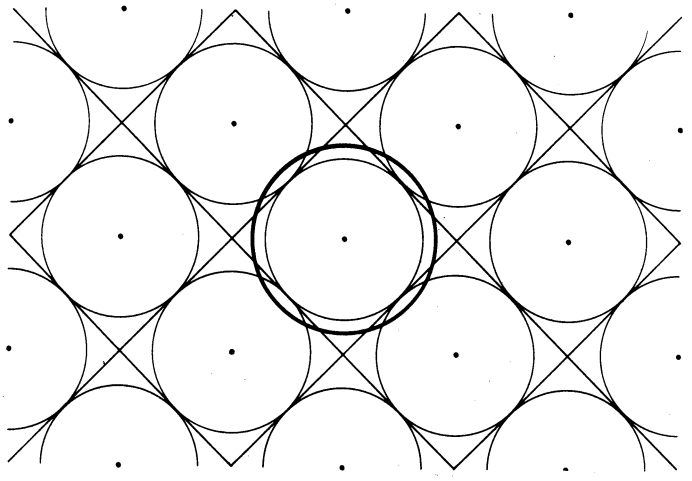

Fig. 2. Atomic cells, muffin-tin spheres and one atomic sphere.

A great simplification arises if proper advantage is taken of the circumstance that the one-electron energies of interest for describing chemical binding are those for which the electron can just about pass, or tunnel through, the potential barrier between the atoms. This means that the wavelength in the interstitial region is much larger than the extent of the region so that by the uncertainty principle the exact value of the wavelength and the detailed shape of the region are irrelevant. In this situation it is a reasonable and most convenient approximation to eliminate the interstitial region through substitution of the muffin-tin spheres by overlapping atomic Wigner-Seitz spheres (Fig. 2), which fill the volume, and to choose the wave-number, κ, for the interstitial region equal to zero. This is the atomic sphere approximation, and it works well for closely packed structures.

The mathematics of the tail-cancellation condition may be written in such a way that it is equivalent to the LCAO formalism but instead of atomic orbitals we have muffin-tin orbitals, $\chi_{tlm}(\vec{R}-\vec{r})$, with tails decaying like multi-pole fields, that is like $|\vec{R}-\vec{r}|^{-l-1}$, and which, inside the spheres, are constructed from the solutions of the radial Schrödinger equations for the crystalline atomic-sphere potential. The subscripts, tlm, on the orbital refer to the relevant type of atom and angular momentum. The effective one-electron Hamiltonian matrix is (17, 22)

$$H_{\vec{R}'l'm';\vec{R}lm} = C_{tl}\delta_{\vec{R}'\vec{R}}\delta_{l'l}\delta_{m'm} + \Delta_{t'l'}^{1/2}S_{\vec{R}'l'm';\vec{R}lm}\Delta_{tl}^{1/2} \qquad (1)$$

which is seen to have the two-centre form (37). The transfer integrals factorize into structure constants, S, which only depend on the positions of the atoms but not on the scale of the lattice, and bandwidth- or overlap-parameters, Δ. The latter,

$$\Delta_{tl} = (1/2)s\chi_{tl}^2(s) = [\mu_{tl}s_t^2(s/s_t)^{2l+1}]^{-1} \qquad (2)$$

is given by the amplitude squared of the radial part of the muffin-tin orbital evaluated at some distance, s, characteristic of the lattice, i.e. s is proportional to the lattice constant, a. The width parameter is furthermore related to an effective electron-mass parameter, μ, as shown in the second part of (eq.2). s_t is the radius of the spheres of type t. The parameters C and Δ, determining respectively the position and width of the band arising from the atoms of type t and angular momentum l, depend on the potential in the appropriate spheres and, in the form given in the present paper, they are slightly energy-dependent (see

Ref. 22, eqs. (11)-(14) and Fig. 2).

Due to our choice of zero wavenumber for the tails of the muffin-tin orbitals the structure constants, S, are just multi-pole expansion coefficients and therefore have an inverse-power-law dependence on the interatomic distance, $R \equiv |\vec{R}'-\vec{R}|$. Through multiplication by the appropriate power of s we achieve that this dependence is on R/s rather than on R and, hence, that the structure constants become independent of the scale, s, of the lattice. Expressed in the usual way as two-centre integrals (37), the transfer integrals are simply

$$\begin{aligned} dd(\sigma,\pi,\delta) &= 10(s/R)^5\Delta_d \quad (-6,4,-1) \\ pd(\sigma,\pi) &= (6\sqrt{5})(s/R)^4(\sqrt{\Delta_p\Delta_d})(-\sqrt{3},1) \\ pp(\sigma,\pi) &= 6(s/R)^3\Delta_p(2,-1) \\ sd\sigma &= (-2\sqrt{5})(s/R)^3(\sqrt{\Delta_s\Delta_d}) \\ sp\sigma &= (2\sqrt{3})(s/R)^2(\sqrt{\Delta_s\Delta_p}) \\ ss\sigma &= -2(s/R)\Delta_s \end{aligned} \tag{4}$$

where the dependence on the lattice constant exclusively enters through the potential parameters, Δ. In this connection it should be noted that, since the atomic spheres are supposed to be space-filling, the sphere radii, s_t, should scale with the lattice constant, i.e. s_t/s should be kept constant.

For a crystal with lattice translations, $\vec{T}$, the structure constants, of course, become

$$S_{\vec{R}'l'm';\vec{R}lm}(\vec{k}) = \sum_{\vec{T}} \exp(i\vec{k}\cdot\vec{T}) S_{\vec{R}'l'm';(\vec{R}+\vec{T})lm} \tag{5}$$

and the Hamiltonian in (eq.1) becomes $H_{\vec{R}'l'm';\vec{R}lm}(\vec{k})$. Here, $\vec{k}$ is the Bloch vector and $\vec{R}$ only denotes atomic positions within the primitive cell.

The factorization seen in (eq.1) into potential parameters and structure constants, and the scale-independence of the latter, lead to the concept of canonical bands. These are just another representation of the structure constants and, hence, they are independent of the potential and the lattice constant; they are characteristics of the crystal structure. Let us first neglect the t'l'-tl hybridizations and define the unhybridized canonical bands: Since the potential parameters only depend on the type, t, of atom and the magnitude, l, of local angular momentum it is obvious that the tl-diagonal block, $H_{\vec{R}'(t)lm';\vec{R}(t)lm}(\vec{k})$, is diagonalized by the same unitary transformation that diagonalizes $S_{\vec{R}'(t)lm';\vec{R}(t)lm}(\vec{k})$. The eigenvalues, $S_{tli}(\vec{k})$, of the latter form the unhybridized canonical tl-band. The unhybridized tl-energy band, $E_{tli}(\vec{k})$, is obtained by centering the canonical band at the energy C_{tl} and scaling it by Δ_{tl}. Specifically, from (eq.1),

$$E_{tli}(\vec{k}) = C_{tl} + \Delta_{tl}S_{tli}(\vec{k}) \qquad i = 1,N_{tl} \tag{6}$$

where i is the subband index and N_{tl} is (2l+1) times the number, N_t, of type t atoms in the primitive cell. It might be reemphasized that C and Δ for s-bands, and to a minor degree for p-bands, are energy-dependent and that (eq.6) therefore may contain a ($\vec{k}$-independent) distortion.

Including now the hybridization it may, for instance, be shown (22) that there exists a canonnical number-of states function, $n(\vec{p})$, which is a characteristic of the crystal structure and in terms of which the tl-projected density of states may be obtained as

$$N_{tl}(E) = (\partial n/\partial p_{tl})(dp_{tl}/dE) \tag{7}$$

Here,

$$p_{tl}(E) \equiv (E-C_{tl})/\Delta_{tl} \tag{8}$$

is the tl-component of the vector $\vec{p}$ and is called the potential function. The spherical average of the electron density in a sphere of type t is

$$n_t(r) = (4\pi N_t)^{-1} \sum_l \int^{E_F} \phi^2_{tl}(E,r) N_{tl}(E)\,dE \tag{9}$$

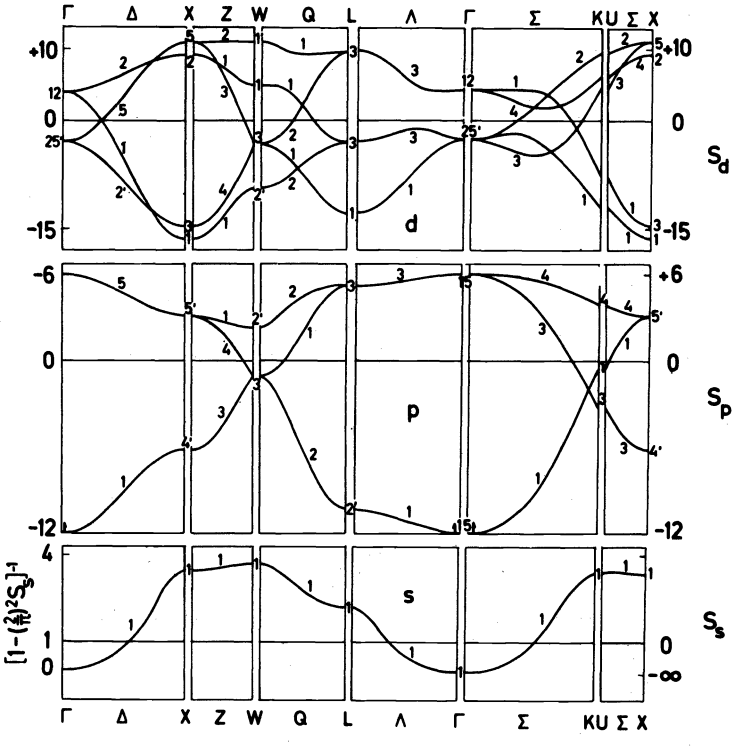

Fig. 3. The unhybridized canonical bands, $S_{li}(\vec{k})$, for the fcc structure.

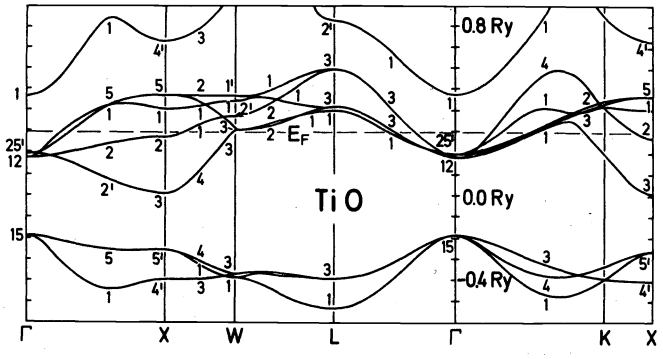

Fig. 4. The energy band structure of TiO at the observed lattice constant.

where ϕ is the solution, normalized to unity in the sphere, of the radial Schrödinger equation. The potential function p, and hence the potential parameters C and Δ, may be expressed in terms of the radial logarithmic-derivative function $s_t\phi'_{tl}(E,s_t)/\phi_{tl}(E,s_t)$ as explained in (Ref. 22, eq. 2).

The Na- and Cl-sublattices in the NaCl-structure are fcc and in Fig. 3 we show the unhybridized canonical s-, p- and d-bands for that structure. For comparison we show in Fig. 4 the fully hybridized energy band structure of TiO. The lowest three bands constitute the O 2p-band which is separated by a gap of about 0.2 Ry from the five Ti 3d-subbands. Above the 3d-band is finally the Ti 4s4p-band. The density of states of TiO is shown in Fig. 5.

Let us first consider the unhybridized d-band in Fig. 3. This is fairly simple to calculate because, according to (eq. 4), the lattice summation in (eq.5) converges after including just a few shells of nearest neighbours, and the only obstacle to performing the calculation by hand for a general $\vec{k}$-point is the diagonalization of a 5x5 matrix. The overall bandwidth, W_d, is trivial to calculate using the expression

$$W_{tl} = (12N_{tl}^{-1} \mid S_{tl}^{tl} \mid^2)^{1/2} \Delta_{tl} \tag{9}$$

involving the second moment, $|S_{tl}^{tl}|^2$, of the density of states for the unhybridized canonical tl-band. The general expression for

$$|S_{t'l'}^{tl}|^2 \equiv \sum_{\vec{R}'m'}^{N_{t'l'}} \sum_{\vec{R}m}^{N_{tl}} \mid S_{\vec{R}'l'm';\vec{R}lm} \mid^2 = |S_{tl}^{t'l'}|^2 \tag{10}$$

is given in (Ref. 22, eq. 22) and it simply yields

$$|S_d^d|^2 = 7000 \sum_{\vec{R}} (s/R)^{10} = 7000 \cdot 12 \cdot (0.3908 \cdot \sqrt{2})^{10} \tag{11}$$

Here, in Fig. 3, and in the following we have chosen the characteristic distance, s, such that it equals the Wigner-Seitz radius of the fcc lattice, i.e.

$$s \equiv (3/16\pi)^{1/3} a = 0.3908\ a \tag{12}$$

where a is the lattice constant. In the evaluation (eq. 11) we have only needed to sum over the 12 nearest neighbours placed at the distance $a/\sqrt{2}$ and, as a result for the fcc sublattice,

$$W_d = 23\ \Delta_d \tag{13}$$

This is in good agreement with the canonical d-bandwidth read off from Fig. 3. The value

TABLE 1. 3d-Bandwidths

	Crystal structure	a (Å)	Δ_d (mRy)	W_d (mRy)	d-Bandextrema (mRy)
Ca	fcc	5.58	13	300	330
Ni	fcc	3.52	11	260	280
CaO	NaCl	4.44	20	460	600
NiO	NaCl	4.27	4.4	100	280

of Δ_d for fcc Ca- and Ni-metal (7) and for Ca- and Ni-monoxide are shown in Table 1. For the metals the lattice constants used are the observed ones but this is not quite true for the monoxides. When going from the metal to the monoxide the lattice constant increases in the case of Ni but it decreases in the case of Ca. This is seen in Fig. 8 . The bandwidth parameter therefore decreases for Ni and increases for Ca. For Ni we realize that the width parameter nearly scales as the lattice constant to the power -5 = -(2l+1). This means that the self-consistent Ni d muffin-tin orbitals in the metal and the monoxide are nearly identical and that the value, $\mu_d = 14$, of the mass parameter (eq. 2) for the metal tabulated in (7) and (16-17) applies to the monoxide as well, provided that the value of s_t in (eq. 2) is set equal to the value of the Wigner-Seitz radius in the metal. For Ca, however, the d-band

in the metal is much more free-electron like than in Ni. In fact $\mu_d = 4.5$ as listed in (7), and from Table 1 we realize that Δ_d nearly scales as the lattice constant to the power -2 which is free-electron scaling.

The d-bandwidth with hybridization neglected, W_d, may now be obtained from (eq. 13) and it is listed in Table 1 together with the hybridized d-bandwidths read off from the extrema of the calculated (nonmagnetic) band structures. It is obvious that, while in the elemental metals the hybridization of the d-band with the metal sp-band has a negligible effect on the d-bandwidth, in the monoxides the covalent hybridization with the O 2p-band increases the d-bandwidth by factors ranging from about 1.3 in CaO to 2.8 in NiO. The profound effect of the O 2p-hybridization on the shape of the metal 3d-band is clearly seen by comparison of the unhybridized d-band in Fig. 3 with the hybridized Ti 3d-band in Fig. 4. In the latter all subbands labelled with the same irreducible representation as an O 2p-subband are pushed up substantially in energy.

In Fig. 6 we show for all the monoxides the extents of our self-consistently calculated (nonmagnetic) bands as functions of the lattice constants. The band extrema are denoted by B (bottom) and T (top) and the potential parameter for the centre of the unhybridized band is, as usual, denoted by C. As we proceed through the series we see how C_d-C_p decreases and that the hybridization pushes the p-band centre below C_p and the d-band centre above C_d. The reason why C_d-C_p decreases through the series is that the d-band falls in energy as it gets filled because the added electron cannot fully screen out the attraction by the added proton. Exactly the same trend is, for instance, observed in the series of elemental transition metals. At the same time as the 3d-band falls in energy the 3d-orbital contracts. Consequently, as we proceed through the series of 3d-monoxides, the width of 3d-band, calculated for a fixed lattice constant, decreases as shown in Fig. 7. Considered at the experimental equilibrium lattice constants the 3d-bandwidth is fairly constant within the group of early- and the group of late monoxides. For a given compound the 3d-bandwidth scales as the lattice constant to a power which varies linearly from -4.0 in ScO to -5.1 in NiO.

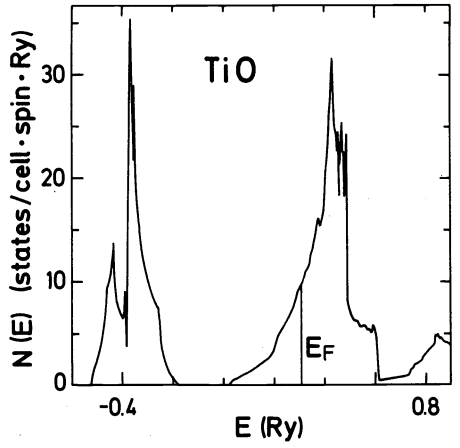

Fig. 5. Density of states in TiO.

We can rather easily estimate the strength of the covalent pd-hybridization: In (eq. 6) the effect of weak t'l'-hybridization is taken approximately into account by addition of the term

$$\sum_{i'}^{N_{t'l'}} |S_{tli,t'l'i'}(\vec{k})|^2 \, \Delta_{tl} \, \Delta_{t'l'} \, (C_{tl}-C_{t'l'})^{-1} \qquad (14)$$

on the right-hand side. This causes the tl-band to shift its position by the amount

$$N_{tl}^{-1} \, |S^{tl}_{t'l'}|^2 \, \Delta_{tl} \, \Delta_{t'l'} (C_{tl}-C_{t'l'})^{-1} \qquad (15)$$

as obtained by performing the average over the Brillouin zone and the N_{tl} subbands labelled by i, and by using the notation in (eq. 10) for the average hybridization structure constant. The value of the latter is readily estimated for the NaCl-structure from the expression given in (Ref. 22, eq. 22):

$$|S^{Md}_{Op}|^2 = 900 \sum_{\vec{R}} (s/R)^8 = 900 \cdot 6 \cdot (0.3908 \cdot 2)^8 = 750 \qquad (16)$$

where $\vec{R}$ now runs over all O positions, measured from one metal position, and we have only included the 6 nearest neighbours at the distance a/2. The values of the combination of poten-

tial parameters entering (eqs. 14 and 15) are

$$\Delta_{Md}\,\Delta_{Op}(C_{Md}-C_{Op})^{-1} = \begin{matrix} 20\cdot 21\cdot 900^{-1}\ \text{mRy} = 0.47 \text{ for CaO} \\ 4.4\cdot 21\cdot 230^{-1}\text{mRy} = 0.40 \text{ for NiO} \end{matrix} \qquad (17)$$

We have here used the values of Δ_d given in Table 1 plus the self-consistently obtained result that Δ_p is 21 mRy in both CaO and NiO, and that the energy difference between the centers of the d- and p-bands is 900 mRy in CaO but only 230 mRy in NiO. By combining the results of (eqs. 15-17) we thus realize that the pd-hybridization pushes the d-band upwards by approximately $5^{-1}\cdot 750\cdot 0.44$ mRy = 70 mRy, and the p-band downwards by approximately $3^{-1}\cdot 750\cdot 0.44$ mRy = 100 mRy, in both CaO and NiO. Hence, the strength of the pd-hybridization, measured in this way, is rather constant through the series.

The inclusion of (eq. 14) as the right-hand side of (eq. 6) not only causes the tl-band to shift but also to widen. The expression for the width of the d-band, obtained by taking second moments like in (eq. 9), now has the form

$$[\, W_{Md}^2 + S_4 \cdot \Delta_{Md}^2\,\Delta_{Op}^2 (C_{Md}-C_{Op})^{-2}\,]^{1/2} \qquad (18)$$

where S_4 is independent of the potential and the lattice constant and involves the fourth moment of the hybridization structure constants. With $S_4 = 5\cdot 10^5$, and using the values of the potential parameters given in Table 1 and (eq. 17), we find that the d-bandwidths including pd-hybridization are 570 mRy in CaO and 300 mRy in NiO. These estimates are in good agreement with the values listed in the last column of Table 1.

The most direct and convenient measure of the strength of the tl-t'l' hybridization is the number of electrons from the entire tl-band which are located in spheres of type t' and there have local angular momentum l'. In the limit of weak hybridization this number is (22)

$$N_{t'l'}^{tl} = 2|S_{t'l'}^{tl}|^2\,\Delta_{tl}\,\Delta_{t'l'}(C_{tl}-C_{t'l'})^{-2} = N_{tl}^{t'l'} \qquad (19)$$

and the factor 2 accounts for the spin-degeneracy. Using the numbers quoted in (eqs. 16-17) we estimate that in CaO the O 2p-band contributes 0.8 electrons with d-character to the Ca-sphere and that in NiO the corresponding number is 2.6. Measured in this way the pd-hybridization thus increases substantially as we proceed through the series of monoxides.

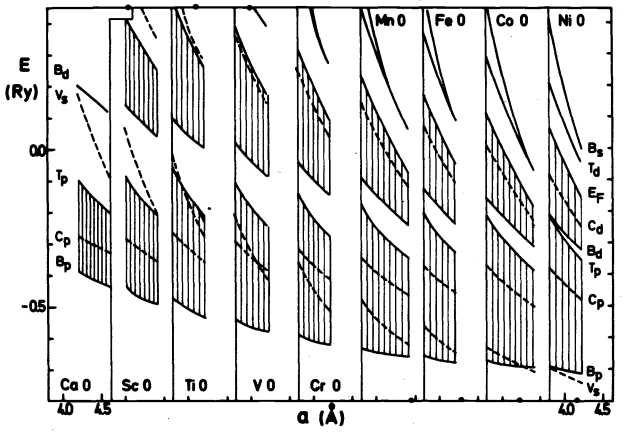

Fig. 6. Self-consistent energy bands for the 3d-monoxides as functions of the lattice constant, a. For each compound the experimental equilibrium lattice constant is indicated on one of the horizontal axes by a black dot. The zero of energy is the electrostatic zero for the infinite crystal. The O 2p-band extends from B_p to T_p, the metall 3d-band from B_d to T_d, and the metal 4s4p-band from B_s and upwards; E_F is the Fermi energy, and occupied bands are shaded. V_s, C_p and C_d are potential parameters: the metal 4s square-well pseudopotential, the O 2p-band centre and the metal 3d-band centre, respectively.

The O 2p-band not only hybridizes significantly with the metal 3d-band but also with the metal s-band. The potential parameter, V_s, indicated in Fig. 6, is the spuare-well pseudopotential for the s-wave in the metal sphere and it is the energy separating the metal 3s- from the

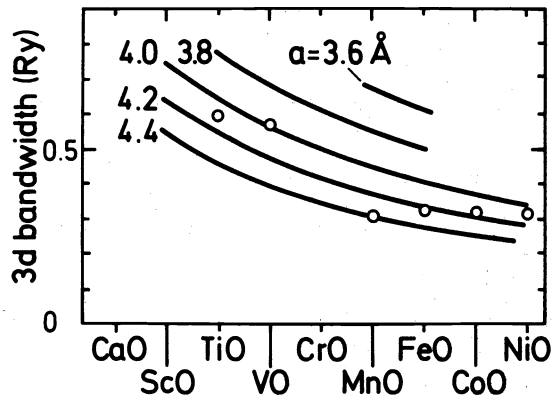

Fig. 7. The variation of the fully hybridized 3d-bandwidth through the series of 3d-monoxides. The dots indicate the widths obtained at the experimental lattice constants.

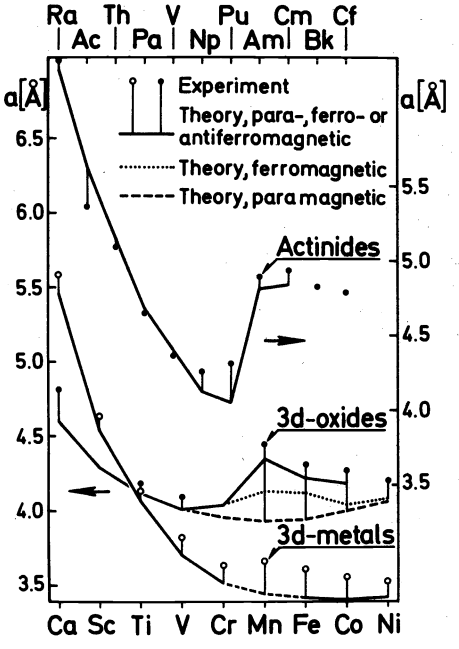

Fig. 8. Comparison of the experimental and theoretical (6-8) equilibrium lattice spacings, a, for the 3d-monoxides and the 3d- and 5f-metals. For the monoxides, having the rocksalt structure, a is the lattice constant while for the elemental metals, having various closely packed crystal structures, a is the lattice constant of the fcc structure with the proper atomic volume.

metal 4s-region in the sense that bands falling below V_s hybridize with the metal 3s-band and bands falling above V_s hybridize with the metal 4s-band. As seen in Fig. 6 the s-pseudopotential approximately follows the same falling trend as C_d. Hence, C_d-V_s is nearly constant through the series of 3d-monoxides while in the elemental 3d-metals it decreases substantially. This difference is caused by the different behaviours of the lattice constants shown in Fig. 8. In the monoxides the covalent hybridization from the metal s-band therefore tends to push the O 2p-band upwards for small lattice constants at the beginning of the series and downwards at the end of the series. (The same is true of the hybridization from the metal p-band.) This is the reason for the increasing downwards shift seen in Fig. 6 of the O 2p-band with respect to C_p as one proceeds through the series.

Due to the long range of the s- and p-orbitals the sp-hybridization is strong in general (see eqs. 4). One of the unhybridized canonical p-bands in Fig. 3 (Δ_1-Λ_1-Σ_1) is seen to be discontinuous at the centre of the Brillouin zone. It may be shown (14) that the discontinuity will always be removed by hybridization with s-waves but the fact remains that this p-subband is extremely soft. If, as in the earliest monoxides, the O 2p-band hybridizes with the lower lying metal 3s-band the soft p-band is pushed upwards and may even lie higher than the other p-subbands near the centre of the zone. If, as in the later monoxides, the O 2p-band hybri-

dizes with the higher lying metal 4s-band the soft p-band is pushed substantially downwards. This is a reason for the increased broadening of the O 2p-band seen in Fig. 6 as we proceed through the series.

The bottom, B_s, of the metal 4s-band (the Γ_1 level in Fig. 4) does not coincide with V_s as in the elemental metals but is pushed near to, or above, the top of the 3d-band by the covalent hybridization with the O 2p-band.

The bandstructures of the ionic insulators CaO and CaS are compared in Fig. 9. In the sulphide the equilibrium lattice constant is larger, Δ_p is larger, C_d-C_p is smaller and the pd-gap is smaller than in the oxide. Therefore, in the sulphide the covalent hybridization is larger and the ionicity smaller than in the oxide. This is borne out even more clearly by comparison

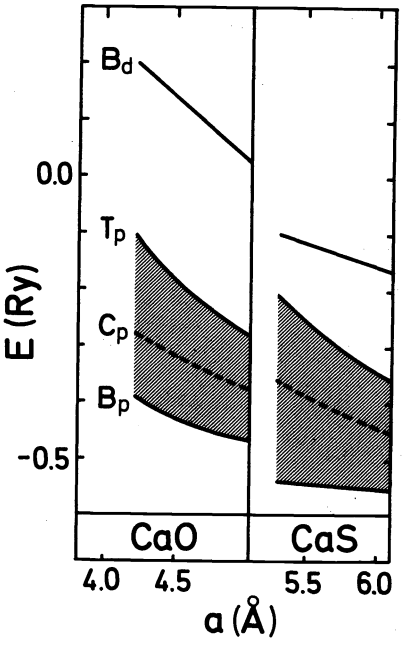

Fig. 9. Self-consistent energy bands of the ionic insulators CaO and CaS as functions of the lattice constant. The experimental equilibrium lattice constants are respectively 4.80 and 5.69 Å.

of the two first panels in Fig. 10. Here we show the number of s-, p- and d-electrons contributed by the chalcogen p-band to the metal sphere. For CaO the number of metal d-electrons was estimated in (eq. 19) and we realize that this number is confirmed by the full calculation. For the ionic compounds where only the chalcogen p-band is occupied the charge, q, of the metal sphere, which equals the excess electronic charge in the chalcogen sphere, is of course given by

$$q = 2 - (N_{Xp}^{Ms} + N_{Xp}^{Mp} + N_{Xp}^{Md}) \qquad (20)$$

and from Fig. 10 we realize that, with our choice of relative sphere sizes, q is about 0.8 in CaO and 0.1 in CaS. This is far from the usual ionic picture, where the charge is 2. As we now proceed from CaO through the series of monoxides we realize that the pd-hybridization, expressed as N_{Op}^{Md}, increases. This was already discussed in connection with (eq. 19) and here we need only point out that for the later monoxides the pd-hybridization is so large that the previously used estimate (eq. 19) becomes very inaccurate; the number of Ni d-electrons contributed by the O 2p-band is 1.3 rather than 2.6. The charge, q, is seen from Fig. 8 to first increase slightly as we proceed from CaO and then after TiO to decrease towards a value of about 0.5 at NiO. This trend is a balanced result of two trends: the increasing covalent hybridization of the O 2p-band, not only with the metal d- but also with the metal sp-band, and the opposing trend caused by the filling of the d-band. The latter trend, which is the weaker, would cause the charge to increase through the series because when the fraction, f, of the d-band is occupied this approximately contributes $f \cdot N_{Xp}^{Md}$ electrons to the oxygen sphere and this contribution should be added on the right hand side of (eq. 20).

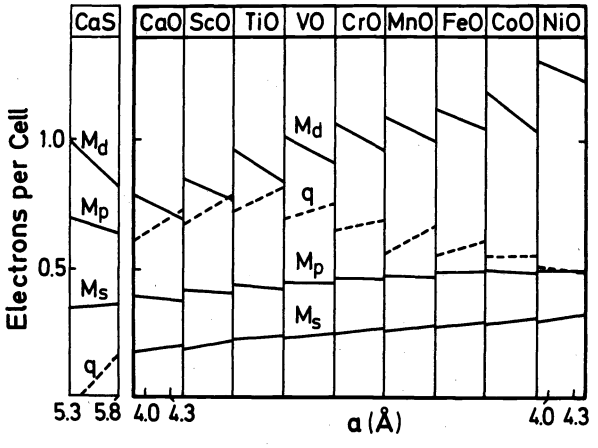

Fig.10. Charge transfer, q, and number of s-, p- and d-electrons contributed to the metal sphere by the chalcogen p-band. The metal and chalcogen spheres were chosen to occupy respectively 62 and 38 per cent of the cell volume.

Until now we have carefully avoided mentioning how we have chosen to share the cell volume, V, between the chalcogen and metal spheres, in other words, how for a fixed s we have chosen s_M/s_X . The structure constants, and hence the canonical bands and number-of-states function, do not depend on this choice but the potential parameters do, to a certain extent. It is obvious that only in such cases, where the calculated energy bands and derived physical quantities are essentially independent of how we chose to share the volume, is the atomic approximation a reasonable one. At the bottom of Fig.11 we show the self-consistently calculated band structure of CaS for a fixed lattice constant and as a function of the relative volume occupied by the Ca sphere, i.e. $V_{Ca}/V = 1-V_S/V$. From this we verify that there is a range around 0.6 where the band structure is essentially independent of V_{Ca}/V. Consistent herewith is our finding that the spherically averaged electron densities are identical at the boundaries of the Ca and S spheres when $V_{Ca}/V = 0.60$. In the upper half of Fig.11 is shown a physical observable to which we shall return in the following section, the pressure, and we realize that the calculated pressure (tot) is nearly constant around $V_{Ca}/V = 0.65$. Similar results have been found for TiO, and these investigations led us to choose $V_M/V = 0.62$ throughout the present work.

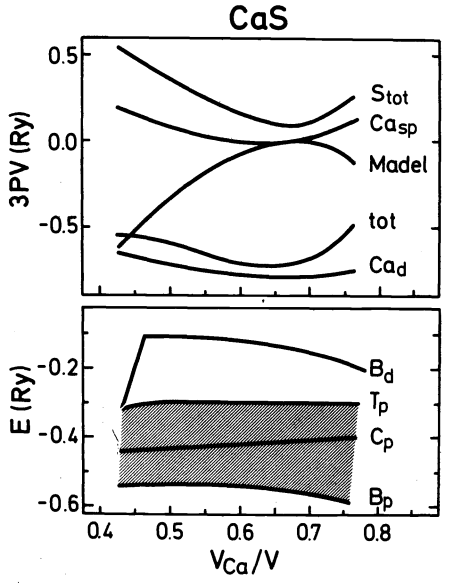

Fig.11. CaS. Partial and total pressures (upper figure) and self-consistent energy bands (lower figure) calculated for different relative sphere sizes, $V_{Ca}/V = 1-V_S/V$, and for constant cell volume, V. (a = 5.69 Å).

Although physical observables calculated with the ASA should be fairly independent of the relative sphere volumes this is of course not so for such quantities as the number of electrons in the various spheres, the charge transfer, q, etc. One might naturally ask whether it would be possible to choose V_{Ca}/V so small that q = 2 whereby our description presumably would come as close as possible to the classical ionic description. In an attempt to do so for CaS we met the difficulty seen in Fig. 11 that for V_S/V exceeding 0.55 the bottom of the S 3d-band moves below the bottom of the Ca 3d-band and hence closes the gap. This might be due to unwarranted approximations in our calculations such as the freezing of the Ca -core and the neglect of the f- and higher partial waves, or it might indicate a breakdown of the ASA for such large sulphur spheres. We are presently investigating these various possibilities and, if the latter turns out to be true, this seems to indicate that, if one insists on a highly ionic ($Ca^{++}S^{--}$) description, then the charge density of the sulphur ion cannot be spherically symmetric.

GROUND-STATE PROPERTIES; ELECTRONIC PRESSURE AND SPIN-POLARIZATION.

In this second part of the paper we shall try to explain how chemical binding or, more specifically, the variation of the total energy with lattice spacing is related to the band structure. In order to calculate the equilibrium lattice constants for the late 3d-monoxides in the present framework we shall find that it is crucial to include the possibility of spin-polarization with the proper antiferromagnetic order.

The basis for our one-electron description of ground-state properties is the density-functional formalism of Hohenberg, Kohn and Sham (2). These authors, quite generally, considered a system of interacting electrons moving in some external potential, v_{ext}, which for instance includes the potential from the nuclei. The Hamiltonian thus comprises the operators for the kinetic energy, the electron-electron interaction and the external potential. Hohenberg and Kohn first showed that, for specified kinetic energy- and electron-electron interaction operators, the ground-state is a unique functional of the electron density, $n(\vec{r})$. It is obvious that if we know the ground-state we can find the density by integrating over all but one of the electron coordinates. The less trivial point is that the density uniquely specifies the external potential, and hence the entire Hamiltonian and thus its ground-state. Since the ground-state is a unique functional of the density, so is the energy, U, of the ground-state (provided it is non-degenerate), and Hohenberg and Kohn secondly showed that the energy functional, $U\{n(\vec{r})\}$, attains its minimum, the ground-state energy, for the proper ground-state density. If we knew the energy functional explicitly we could thus rather easily estimate the ground-state energy and density be seeking the minimum of the functional for various trial densities. However, the energy functional is not known and the complexity of the many-electron problem is associated with its determination.

Guided by the success of the one-electron picture, going back to Bohrs explanation of the periodic system of the elements and including the recent use of Slaters $n(\vec{r})^{1/3}$-exchange for one-electron calculations in atoms and solids, Kohn and Sham proposed to write the energy functional in a form for which the minimalization proceedure leads to a self-consistent one--electron problem: Together with the system of real electrons they considered a system on non--interacting electrons moving in an external potential, $v(\vec{r})$. For $v(\vec{r})$ specified, the corresponding one-electron Schrödinger equation may be solved and it yields the one-electron states, $\psi_j(\vec{r})$, and energies E_j. The ground-state for the system of non-interacting electrons is then the Slater determinant obtained by occupying the lowest-lying one-electron states, the density is

$$n(\vec{r}) = \sum_j |\psi_j(\vec{r})|^2 \tag{20}$$

and the kinetic energy is

$$T = \sum_j \langle\psi_j| -\nabla^2 |\psi_j\rangle = \sum_j E_j - \int v(\vec{r}) n(\vec{r}) d^3r \tag{21}$$

By application of the Hohenberg-Kohn theorem to the non-interacting system one can always find an external potential, $v(\vec{r})$, which through the above-mentioned proceedure will generate a specified ground-state density, $n(\vec{r})$. This density may therefore be used as the trial density for the system of properly interacting electrons and, for the latter, Kohn and Sham now expressed the energy functional as

$$U\{n(\vec{r})\} = T\{n(\vec{r})\} + G\{n(\vec{r})\} \tag{22}$$

where $T\{n(\vec{r})\}$ is given by (eq. 21). The non-interacting systems are thus used to generate trial densities for the proper system and to define a kinetic energy term, T, of the functional (eq. 22). The second term, G, is the sum of the interaction with the external potential (the nuclei)

$$\int v_{ext}(\vec{r}) n(\vec{r}) d^3r \tag{23}$$

the classical Coulomb interaction energy

$$(1/2)\iint 2|\vec{r}'-\vec{r}|^{-1} n(\vec{r}')n(\vec{r})d^3r'd^3r \tag{24}$$

and a remainder, the so called exchange-correlation energy functional,

$$E_{xc}\{n(\vec{r})\} \tag{25}$$

This is the sum of two differences: the difference between the kinetic energy functional of the proper system and that (eq. 21) of the non-interacting system, and the difference between the true electron-electron interaction energy and that (eq. 24) of the electronic charge clouds. The many-elctron problem is thus hidden in the exchange-correlation part of the energy functional. We may now try to adjust the one-electron potential, $v(\vec{r})$, in such a way that the density generated through (eq. 20) minimizes the energy functional (eq. 22) and, hence, equals the ground-state density. This leads to the self-consistency condition

$$v(\vec{r}) = -\delta T\{n(\vec{r})\} / \delta n(\vec{r}) =$$

$$\delta G\{n(\vec{r})\} / \delta n(\vec{r}) = v_{ext}(\vec{r}) + \int 2|\vec{r}'-\vec{r}|^{-1} n(\vec{r}')d^3r' + \delta E_{xc}\{n(\vec{r})\} / \delta n(\vec{r}) \tag{26}$$

where we have used (eq. 21) in the first equation, (eq. 22) in the second and (eqs. 23-25) in the third. On the right-hand side the first two terms are the Coulomb potentials from the nuclei and the electronic charge cloud and the third term is the (unknown) exchange-correlation operator.

In the present calculation we have used the following local approximation to the exchange--correlation energy functional

$$E_{xc}\{n(\vec{r})\} = \int \varepsilon_{xc}(n(\vec{r}))n(\vec{r})d^3r \tag{27}$$

with $\varepsilon_{xc}(n)$ being the estimate given by Hedin and Lundqvist (3) of the exchange plus correlation energy per electron for a homogeneous electron gas of density n. This approximation is exact in the limit of slowly varying densities and, in contrast to the Thomas-Fermi approximation, it is also correct in the limit of high densities because there it includes the kinetic energy correctly. In the so called local spin-density scheme (3) the exchange-correlation energy density in (eq. 27) is substituted by $\varepsilon_{xc}(n\uparrow,n\downarrow)$ which applies to a homogeneous electron gas with density, $n \equiv n\uparrow + n\downarrow$, and spin density, $m \equiv n\uparrow - n\downarrow$, as created by an external magnetic field. In the local approximation the operator $\delta E_{xc}/\delta n$ is an ordinary potential

$$v_{xc}(\vec{r}) = d[n\varepsilon_{xc}(n)]/dn \equiv \mu_{xc}(n(\vec{r})) \tag{28}$$

namely the exchange-correlation part of the chemical potential in a homogeneous electron gas. The exchange-only part of this potential is proportional to the cube root of the density and equals the so called Xα-potential with $\alpha = 2/3$.

It should be emphasized that the self-consistent one-electron scheme presented above is designed to yield ground-state properties such as the total energy and the electron (and spin) density. The many-electron wavefuction is not aimed at. Rather, the effects of exchange and correlation are built into the energy functional and the one-electron energies and wavefunctions have no direct meaning. Nevertheless, as we shall show in the following, they are useful concepts for understanding cohesive and magnetic properties. Energies and lifetimes of quasiparticle excitations, on the other hand, should be obtained from a one-electron equation containing the Dyson self-energy operator instead of $\delta E_{xc}/\delta n$ but, at the Fermi level, these two are identical and the Fermi surface obtained in a ground-state calculation is therefore the correct one.

The ground-state energy in the local approximation is seen to be

$$U = \sum_j E_j - (1/2)\iint 2|\vec{r}'-\vec{r}|^{-1} n(\vec{r}')n(\vec{r})d^3rd^3r'$$

$$+ \int[\varepsilon_{xc}(n(\vec{r}))-\mu_{xc}(n(\vec{r}))]n(\vec{r})d^3r + (1/2)\sum_{R'\neq R}\sum 2|\vec{R}'-\vec{R}|^{-1} Z\,Z' \tag{29}$$

in terms of the self-consistent one-electron energies and density and where we have included the repulsion between the nuclei. We are not particularly interested in the total energy but rather in differences between total energies as we change the positions of the atoms. In such differences large energies associated with the core electrons cancel and the sum of the one--electron energies is substantially reduced by the double-counting terms in (eq. 29). We shall now show that, for an infinitesimal change of the atomic positions, the change of the total energy, that is the force on the nuclei, may be expressed as the electrostatic force between atomic cells plus the change in the sum of the valence-electron energies for rigidly shifted cellular potentials (17). Hence by considering the force rather then the total energy, the problems associated with core-electrons and double-counting are avoided and a conceptually

simple picture emerges.

For the sake of the argument we consider a diatomic molecule. Suppose that we have solved the one-electron problem self-consistently for the internuclear distance, R, and have obtained the one-electron energies and -potential, v^{sc}, as well as the ground-state density, n^{sc}, and -energy, $U\{n^{sc}\}$. For later use it will proove practical to imagine a cut between the nuclei which divides space into two atomic cells, a and b. The potential and the density have thus been cut into the cellular functions

$$v_a^{sc}(\vec{r}_a), \quad v_b^{sc}(\vec{r}_b), \quad n_a^{sc}(\vec{r}_a) \text{ and } n_b^{sc}(\vec{r}_b), \tag{30}$$

where $\vec{r}_a$ and $\vec{r}_b$ are local coordinates centered at the nuclei. Let us now increase the distance between the nuclei by dR and ask for the first-order change of the total energy, that is the inter-nuclear force. This may be estimated as

$$dU = U_{R+dR}\{n_{R+dR}\} - U_R\{n_R^{sc}\} \tag{31}$$

where, by virtue of the stationary property of the energy functional, the trial density for the distorted system may differ to first order from the self-consistent density for that system. The trial density we obtain from (eq. 20) by solving Schrödingers equation for a potential which equals the rigidly shifted ones in cells a and b (eq. 30) and equals their continuous interpolation into the cut which has now been opened up. The kinetic-energy contribution to (eq. 31) is then

$$\delta T = \delta \sum_j E_j - \int_a v_a^{sc}(\vec{r})\delta n_a(\vec{r})d^3r - \int_b v_b^{sc}(\vec{r})\delta n_b(\vec{r})d^3r - \int_{cut} v^{sc}(\vec{r})n^{sc}(\vec{r})d^3r \tag{32}$$

as may be seen from (eq. 21) by breaking the integral over all space into integrals over cells plus an integral over the infinitesimal cut-region. We have used the symbol, δ, instead of,d, to indicate changes which correspond to the rigidly shifted, rather than self-consistently relaxed, one-electron potential. The contribution to (eq. 31) from the term G in (eq. 22), now including the internuclear repulsion, may be divided into three terms arising from: 1) the density changes δn_a and δn_b, 2) the change of the nuclear positions entering the electron-nuclear and internuclear interactions, and 3) the integrals over the cut-region. The double-counting term 1) simply cancels the second and third terms in (eq. 32) because $v^{sc} = \delta G/\delta n$ according to (eq. 26). The term 2) is the electrostatic force between the charge densities in cells a and b, and 3) is a surface integral. We therefore obtain the so called force-relation (17):

$$dU = \delta \sum_j E_j + \text{intercellular electrostatic force} \cdot (-dR)$$
$$+ \int_{cut} [\varepsilon_{xc}(n(\vec{r})) - \mu_{xc}(n(\vec{r}))]n(\vec{r})d^2r dR \tag{33}$$

The total force, of course, only depends on the virtual displacement of the nuclei and, where in the region between the nuclei we choose to make the cut, only effects the relative weight of the three terms in (eq. 33). If the cut is made right around one nucleus only the electrostatic term survives; this is the well-known (rather impractical) Hellmann-Feynman result. If, on the other hand, we make the cut through regions of low electron density the electrostatic term is relatively simple to compute and only the energies of the valence electrons enter the one-electron energy term. The use of a rigidly shifted potential ensures that the chemical shift of the core-electron energies and, as previously mentioned, the double-counting term do not enter the force relation.

We now wish to consider an infinite crystal and study the change of the total energy for a uniform expansion; this is the electronic pressure:

$$P \equiv - dU / dV \tag{34}$$

We here neglect the contribution from the zeropoint motion. The pressure-volume relation, P(V), which is shown schematically in Fig. 12, is the equation of state at zero temperature. In terms hereof the equilibrium cell volume, V_{eq}, is determined by

$$P(V_{eq}) = 0 , \tag{35}$$

the bulk modulus, or inverse compressibility, by

$$B = - dP / d\ln V \Big|_{V_{eq}} , \tag{36}$$

and the cohesive energy per cell by

$$U_{coh} = -\int_{V_{eq}}^{\infty} PdV = -\int_{0}^{\infty} 3PV\, d\ln(a/a_{eq}) \tag{37}$$

The force relation yields a most useful expression for the pressure if we perform the cuts along the boundaries of, suitably chosen, atomic cells. Furthermore, in the atomic sphere approximation, the differentiation with respect to the lattice constant of the one-electron energies may be performed analytically because the structure constants are independent of the lattice constant.The electrostatic term just yields the usual monopole Madelung term because the charge densities are spherically symmetric.

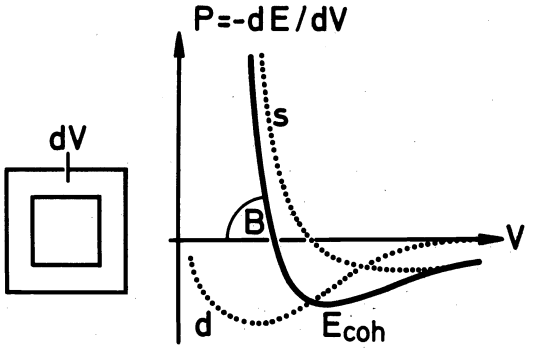

Fig. 12. Equation of state and partial s- and d-pressures for a typical transition metal.

In the preceeding chapter we introduced the ASA as an approximate scheme for performing self-consistent one-electron calculations. The approximate energy functional which leads to a self-consistent ASA calculation is, in fact, given by

$$T^{ASA} = \int^{E_F} EN(E)dE - \sum_{\vec{R}\,t} \int v_t(r) n_t(r) d^3r \,, \tag{38}$$

where N is the density of states per cell calculated in the ASA, the sum is over all atomic spheres in the primitive cell and the integral is in a sphere of type t. Moreover,

$$G^{ASA} = (1/2) \sum_{\vec{R}} \sum_{\vec{R}'} (-S_{\vec{R}\vec{R}'}/s) q_t q_{t'} - \sum_{\vec{R}\,t} \int 2r^{-1} Z_t n_t(r) d^3r$$
$$+ (1/2) \sum_{\vec{R}\,tt} \iint |\vec{r}'-\vec{r}|^{-1} n_t(r') n_t(r) d^3r d^3r' + \sum_{\vec{R}\,t} \int \varepsilon_{xc}(n_t(r)) n_t(r) d^3r \tag{39}$$

Here, $S_{\vec{R}\vec{R}'}$ is an ss-structure constant in the limit of zero Block vector, i.e. a Madelung constant.

We now evaluate the pressure relation (eq. 33) in the ASA and first consider the change in the sum of the one-electron energies for a uniform expansion of the lattice. In terms of the integrated density-of-states function, n(E), we obtain by partial integration

$$\delta \int^{E_F} EN(E)dE = \delta\,[E_F n - \int^{E_F} n(E)dE] = -\int^{E_F} [\delta n(E)]dE \tag{40}$$

because the total number of electrons, $n(E_F)$, is constant. The structure constants and hence the canonical number-of-states function, defined in connection with (eq. 7), are independent of the scale of the lattice; only the potential functions in (eq. 8) depend hereon. Consequently

$$\delta \int^{E_F} EN(E)dE = -\int^{E_F} \sum_{tl} (\partial n/\partial p_{tl})\, \delta p_{tl}(E)\, dE \tag{41}$$
$$= \sum_{tl} \int^{E_F} [\delta C_{tl} + (E-C_{tl}) \delta \ln \Delta_{tl}]\, N_{tl}(E)dE = \sum_{tl} n_{tl}\, [\delta C_{tl} + (\bar{E}_{tl} - C_{tl}) \delta \ln \Delta_{tl}]$$

In the second equation we have neglected the energy dependence of the potential parameters, which is a reasonable approximation for narrow p-, d-, and f-bands, and the change of the energy bands is therefore simply the sum of a term involving the change of the potential parameter for the centre of the band and a term involving the change of the bandwidth parameter. (The exact expressions may be found in (17-18)) The ASA pressure-relation is thus

$$3PV = -\sum_{tl} n_{tl}\,[\delta C_{tl}/\delta \ln s_t + (\bar{E}_{tl}-C_{tl})\delta \ln \Delta_{tl}/\delta \ln s_t] + U_{MDL}$$

$$= \tfrac{2}{3}\,[\sum_{tl} P_{tl} + P_{MDL}]\,V \qquad (42)$$

which shows how the total pressure may be written as a sum of partial pressures. The electrostatic term is the Madelung energy because it is inversely proportional to the lattice constant and therefore

$$[3PV]_{MDL} = -\delta U_{MDL}/\delta \ln a = U_{MDL} \qquad (43)$$

Furthermore, the surface term of (eq. 33) has been included in the one-electron term in (eq. 42) as will be explained below.

The dependence of the potential parameters on the lattice constant and hence on the sphere radius, s_t, for a rigid atomic-sphere potential is simply given by the radial Schrödinger equation for that potential. Outside its sphere a muffin tin orbital decays as if the kinetic energy, $C-v(\vec{r})$, were zero. The change of the orbital energy, C, as the sphere size is increased is therefore

$$\delta C = \int_{s_t}^{s_t+ds_t} [-C+v(r)]\,\chi^2(r)r^2dr = -[C-v(s_t)]\,\chi^2(s_t)s_t^2ds_t \qquad (44)$$

by first order perturbation theory. For the purpose of substitution in (eq. 42) we must include the surface term of (eq. 33) and hence

$$\delta C_{tl}/\delta \ln s_t = -[C_{tl} - v_t(s_t) + \mu_{xc}(n_t(s_t)) - \varepsilon_{xc}(n_t(s_t))]\,2\mu_{tl}^{-1} \qquad (45)$$

The value of $\varepsilon_{xc} - \mu_{xc}$ at the sphere boundary is of the order of 0.2 Ry. This is so because, neglecting correlation, $\varepsilon_x - \mu_x = -\mu_x/4$ and, by assuming that the exchange-correlation hole is spherically symmetric and centered at the nucleus, $\mu_{xc} = -2/s_t$. In (eq. 45) we have used the expression for the band mass (not to be confused with the exchange-correlation potential) given in (eq. 2). For the width parameter, defined in the same equation, we find

$$\delta\Delta_{tl} / \delta \ln s_t = 1 + 2\delta\chi_{tl}(s)/\delta \ln s = -(2l+1) - 2\mu_{tl}^{-1} + \ldots \qquad (46)$$

The first term is due to the r^{-l-1} decay of the muffin-tin orbital, the second is the correction due to the renormalization of the orbital to the larger sphere, and the third is due to the correction of the orbital curvature on the sphere boundary. This third term, proportional to $C-v+\mu_{xc}-\varepsilon_{xc}$, may be found in (17-18).

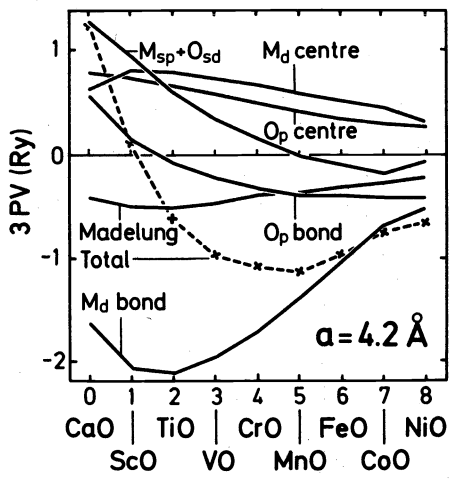

Fig. 13. Partial pressures in the 3d-monoxides calculated for the paramagnetic phases and the lattice constant 4.2 Å. The relative sphere volumes were chosen as in Fig. 10.

The partial pressures in the 3d-monoxides calculated for the paramagnetic phase and the lattice constant 4.2 Å are shown in Fig. 13. These results as well as those shown in the other figures of the present paper were obtained including the proper energy dependence of Δ in (eq. 8). In

Fig. 13 the metal d- and O p-partial pressures have been separated into their respective centre (C) and bond (Δ) contributions. The centre contributions are seen to be positive, that is repulsive, and this means that the energies, C, under compression move upwards with respect to the rigid potential. For paramagnetic NiO we find, by evaluation of (eq. 45) that

$$\delta C_d/\delta \ln a = -260 \text{ mRy} \cdot 2 / 14 = -37 \text{ mRy} \quad (47)$$

and by comparison with Fig. 6 this is seen to be about 50 times smaller than the derivative dC/dlna, which includes the self-consistent relaxation of the one-electron potential. Had we thus based our pressure relation on the self-consistent changes of the one-electron energies the double-counting terms would have been almost as large but of opposite sign. In NiO there are 8.6 electrons with d-character in a Ni-sphere and we therefore obtain a repulsion of about 0.32 Ry as shown in Fig. 13. The d-centre contribution is seen to decrease from CaO to NiO although the number of d-electrons in the metal sphere increases from 0.70 in CaO, where they are all contributed by the O 2p-band, to 8.6 in NiO, where the 1.3 hereof are contributed by the O 2p-band. This is because $C-v+\mu_{xc}-\varepsilon_{xc}$ falls from 1.05 to 0.26 Ry and because the d-mass increases from 2.7 to 14. The upwards movement of the O p-centre under compression is given by

$$\delta C_p/\delta \ln a = -110 \text{ mRy} \cdot 2 / 3.5 = -63 \text{ mRy} \quad (48)$$

in paramagnetic NiO, and this is about 20 times smaller than the self-consistent change seen in Fig. 6. With 4.3 p-electrons in the O-sphere this yields the repulsion of 0.26 Ry seen in Fig. 13. The repulsion from the O p-centre falls through the series because $C-v+\mu_{xc}-\varepsilon_{xc}$ falls from 0.26 to 0.11 Ry; the O p-mass and the number of p-electrons in the O-sphere are rather constant.

A bond-contribution to the pressure is negative, that is attractive, provided that the occupied centre of gravity, $\bar{E}$, lies below the potential parameter, C; in other words, that relatively to C there are more bonding than antibonding states occupied. This is so because the band always widens under compression, as expressed by (eq. 46). Therefore all states below C, the bonding states, fall in energy relatively to C while those above C, the antibonding states, rise their energy relatively to C. For the dependence of the metal d- and O p-bandwidth parameters, Δ, on the sphere radius we find powers close to respectively -5 and -3 for rigid, (eq. 46), as well as for self-consistently relaxed potentials.

The O 2p-band is full for all the monoxides and were it not for hybridization effects and distortion of the p-band due to a slight energy dependence of Δ_p (see (22), Fig. 2) the O p-bonding pressure would be zero. As seen in Fig. 6, in CaO the major part of the p-band lies above C_p due to the energy dependence of Δ_p, and the O p-bonding pressure is therefore slightly positive. As we proceed through the series the O 2p-band starts to hybridize with the unoccupied metal 4s- and 4p-bands. This pushes the O 2p-band downwards with respect to C_p, so much, that the O p-bond pressure eventually becomes negative. This effect is somewhat weakened by the filling of the metal d-band which causes an occupation of the antibonding O p-projected state density in the d-band region far above C_p. In order to discuss the metal d-bonding pressure let us consider a simplified model for the effects of pd-hybridization and d-band filling.

We assume that the p- and d-bands have rectangular, non-overlapping densities of states which without pd-hybridization would be centered at respectively C_p and C_d. The d-bandwidth, including the hybridization-broadening considered in (eq. 18), is W_d. The p-band can hold $N_p = 6$ electrons of which $N_p - N_{pd}$ are p-projected electrons in the O-sphere and N_{pd} are d-projected electrons in the metal sphere. Similarly, the d-band can hold $N_d = 10$ electrons of which $N_d - N_{pd}$ are d-electrons in the metal sphere and N_{pd} are p-electrons in the O-sphere. N_{pd} is given by (eq. 19) and measures the strength of the hybridization. In terms hereof, and according to (eq. 15), the displacements of the p- and d-bands are respectively $(C_p-C_d)N_{pd}/N_p$ and $(C_d-C_p)N_{pd}/N_d$.

In the case of CaO the p-band is full and the d-band is empty. The centre of gravity of the p-band, the occupied p-projected, and the occupied d-projected state densities therefore coinside and lie lower than C_p by the amount $(C_d-C_p)N_{pd}/N_p$. According to (eq. 42) this sets up the p-bond pressure

$$[3PV]^{f=0}_{\text{p-bond}} = -N_p(C_p-C_d)(N_{pd}/N_p)(-3) = -3N_{pd}(C_d-C_p)$$
$$= -3 \cdot 0.7 \cdot 0.9 \text{ Ry} = -1.9 \text{ Ry for CaO} \quad (49)$$

The p-bond pressure in Fig. 13 is slightly possitive due to the above-mentioned additional effects. In (eq. 49) and in the following we only work to first order in the hybridization. The d-bond pressure in our simplified model is

$$[3PV]^{f=0}_{d\text{-bond}} = -N_{pd}(C_p-C_d)(-5) = -5N_{pd}(C_d-C_p)$$
$$= -5\cdot 0.7\cdot 0.9 = -3 \text{ Ry for CaO} \quad (50)$$

which compared with the result in Fig. 13 is somewhat too attractive.

We now start to fill the d-band. If the fractional d-band occupancy is f, then the occupied centre of gravity for the d-band lies $(1-f)W_d/2$ below the centre of the d-band and the number of p-and d-projected electrons in the d-band is fN_{pd} and $f(N_d-N_{pd})$ respectively. The p-bond pressure will, in addition to the bonding contribution (eq. 49) from the p-band, have an antibonding contribution from the d-band and the sum of these is

$$[3PV]_{p\text{-bond}} = -3N_{pd}\,[(W_d/2)f + (C_d-C_p)]\,(1-f) \quad (51)$$

The contibution from the d-band increases with the filling and eventually cancels the p-band contribution. This trend was mentioned previously. The d-bonding pressure will, in addition to the contribution (eq. 50) from the p-band, have a bonding contribution from the d-band and the sum of these is

$$[3PV]_{d\text{-bond}} = -5\,[(N_d-N_{pd})(W_d/2)f + N_{pd}(C_d-C_p)]\,(1-f) \quad (52)$$

As a function of the d-band filling, and for constant potential parameters, the trend followed by the d-bond pressure is parabolic. Without hybridization the trend is symmetric with minimum for a half-full band and zero for empty and full bands. This is the trend found in calculations for the elemental 3d-metals as shown in Fig. 14. In the presence of hybridization the parabola is skew. The pressure still vanishes for f=1 but it is negative for f=0, as we have seen in (eq. 50). The minimum occurs for

$$f = 0.5 - (C_d-C_p)(N_{pd}/N_d)W_d^{-1} = 0.5 - 0.5\cdot(1/10)\cdot 0.5^{-1} = 0.4, \text{ for CrO} \quad (53)$$

The minimum is thus displaced by an amount equal to the ratio between the hybridization shift and the width of the d-band. For the 3d-monoxides the decrease of the d-bandwidth shown in Fig. 7 causes the minimum to be further displaced as is seen in Fig. 13. We may conclude by adding (eq. 51) and(eq. 52). We thereby obtain the result that the pressure created by the metallic dd-bond is approximately

$$[3PV]_{dd\text{-bond}} = -25\,W_d\,f\,(1-f), \quad (54)$$

where we have neglected a small term proportional to N_{pd} and where W_d includes the indirect dpd-interaction met in (eq. 18). In addition, the pressure created by the pd-covalent bond is approximately

$$[3PV]_{pd\text{-bond}} = -8N_{pd}(C_d-C_p)(1-f) \quad (55)$$

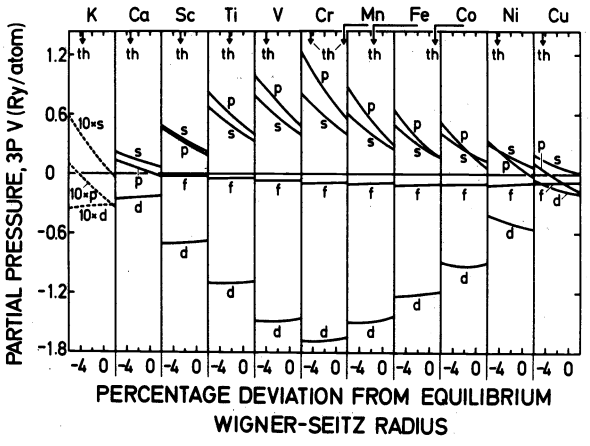

Fig. 14. Partial pressures calculated (7) for the elemental 3d-metals as functions of the Wigner-Seitz radius. The experimental and theoretical (th) equilibrium lattice constants are shown in Fig. 8.

We have sofar not discussed the Madelung and the metal sp- and O sd-pressures shown in Fig. 13. The Madelung pressure, (eq. 43), equals

$$[3PV]_{Mad} = \alpha q^2/a \ , \tag{56}$$

where α is the Madelung constant, and it therfore follows the slowly decreasing trend of the charge transfer discussed in connection with Fig. 10.

The metal s- and p-, and the O s- and d-bands lie far outside the region of interest and those bands which are occupied are so narrow that they do not contribute to the pressure. The metal sp- and O sd-pressures therefore arise from the corresponding projected densities of states in the region of the O 2p-band and the occupied part of the metal 3d-band. The potential functions of these partial waves, which are only used to augment the tails of the O 2p- and metal 3d-orbitals inside neighbouring spheres, do not follow (eq. 8) but rather, (14,22),

$$p_{tl}(E) = \Gamma_{tl} \ / \ (V_{tl}-E), \tag{57}$$

where V is the square-well pseudopotential met in connection with Fig. 6, and where approximately

$$\Gamma_{tl} = 2(2l+1)^2(2l+3)s_t^{-2}(s/s_t)^{2l+1} \tag{58}$$

The corresponding partial pressures are given by

$$[3PV]_{tl} = -n_{tl}\,[\delta V_{tl}/\delta \ln s_t + (\bar{E}_{tl}-V_{tl})\delta \ln \Gamma_{tl}/\delta \ln s_t] \tag{59}$$

where

$$\delta V_{tl}/\delta \ln s_t = -(2l+3)(V_{tl}-v+\mu_{xc}-\varepsilon_{xc}) \tag{60}$$

and

$$\delta \Gamma_{tl}/\delta \ln s_t = -2 \tag{61}$$

There are very few O s- and d-electrons and the corresponding partial pressures may therefore be neglected. As seen in Fig. 10 the number of metal s- and p-electrons is about 0.2 and 0.4 in CaO and these numbers increase slightly through the series. The metal s- and p-pseudopotentials are nearly equal and follow the trend shown in Fig. 6. For the sake of the argument we may consider the metal p-pressure only and neglect the second term in (eq. 59). For CaO we then find

$$[3PV]_{Ca\ p} = -0.4\ (-5{\cdot}1\ Ry) = 2\ Ry \tag{62}$$

which by comparison with Fig. 13 is seen to have the correct order of magnitude. As we now proceed through the series of 3d-monoxides the metal cores shrink and the pseudopotential falls drastically in energy as shown in Fig. 6. The metal sp-pressure falls accordingly and even changes sign when the covalency between the metal 4s4p-band and the O 2p-band starts to develop. This explains the trend seen in Fig. 13.

Having discussed all the partial pressures we may sum them up and obtain the total pressure shown in Fig. 13. This total pressure, evaluated at the same lattice constant for all the monoxides, must follow the same trend as the equilibrium lattice constant (eq. 35), provided that the bulk modulus (eq. 36) does not change too much. This is indeed the case as may be seen by comparison of Figs. 13 and 1. The equilibrium lattice constants in Fig. 1 were obtained by computing the pressure as a function of the lattice spacing and the results of such a series of self-consistent calculations are shown in Figs. 15 and 16. We shall return to the effects of magnetism (AF) in a moment, and for the non-magnetic (P) bands the dependence of the pressure on the lattice spacing may be explained in the same way as we explained the trends through the series in terms of the band structures and occupancies shown in Figs. 6, 7 and 10.

In conclusion, the pd-covalent bond, the dd-metallic bond and the ionic bond provide a soft attraction which is counter-balanced by a stiff repulsion caused by the volume-dependence of the centres of the O p- and metal d-bands and the metal 3s3p-core. As the metal d-band is filled up the attraction from the pd-covalent and the dd-metallic bonds weaken. At the same time the repulsion from the metal 3s3p-core changes into a metal 4s4p - oxygen 2p covalent attraction. The ionic bond remains rather constant through the series. The trend followed by the lattice constants of the non-magnetic 3d-monoxides shown in Fig. 1 is the result of the parabolic trend followed by the pd-covalent and dd-metallic attraction, expressed in (eqs. 54 and 55), and the strongly decreasing trend followed by the metal sp-pressure. The fact seen in Fig. 8 that the (calculated, paramagnetic) minimum lattice constant occurs at MnO (f=0.5) in the series of monoxides while at Co (f=0.9) in the series of elemental 3d-metals is an effect of covalency. Compared with the common picture of bonding in the 3d-monoxides the one presented here is far more covalent and far less ionic. By choosing larger chalcogen and smaller metal spheres it is possible to shift the weight towards the ionic picture but we doubt whether a fully ionic ASA description is possible.

In the present paper we have only considered how the total energy depends on one degree of freedom, namely the scale of the lattice, and our separation of the total pressure into partial pressures was done merely because we felt that the trends followed by the partial pressures were simple to understand. We must therefore warn against interpreting the partial pressures as individual pressures. For instance does the fact that the chalcogen pressure is positive and the metal pressure negative not mean that the total energy is lowered if the chalcogen cell is expanded and the metal cell contracted. The total energy is, of course, independent of the relative cell sizes; it only depends on the positions of the nuclei. Another point worth mention is that, whereas the total pressure is independent of the relative cell sizes (in the ASA, nearly independent), this does not hold for the partial pressures. The relative weight given in our description to various terms such as core repulsion and ionicity therefore to some extend depend on the choise of sphere sizes. This is illustrated in the upper part of Fig. 11.

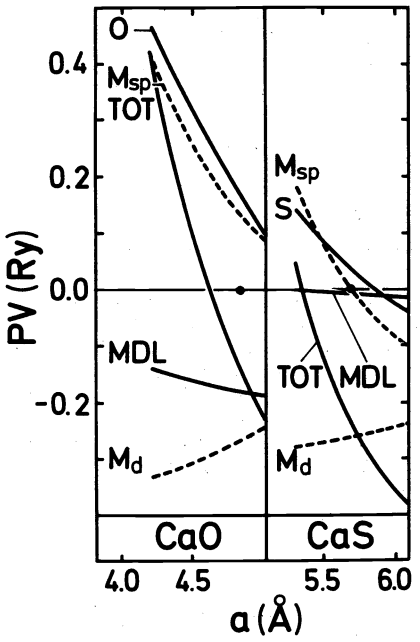

Fig. 15. Partial and total pressures of the ionic insulators CaO and CaS calculated as functions of the lattice constant. $V_{Ca}/V=0.62$.

We see from Fig. 1 that the anomalous large lattice constants found in the second part of the series of monoxides are not reproduced by the non-magnetic band structures considered so far and we shall therefore include the possibility of spin-polarization. The density-functional formalism can, in principle, yield a ground state with net spin but, in practice, this requires an approximation far more sophisticated than the local approximation expressed by (eq. 27). It is a rather simple matter, however, to generalize the formalism to a spin-density formalism (3) in which the element $n(\vec{r}\sigma,\vec{r}\sigma')$ of the density matrix is the independent variable and in which the external potential has the form $v_{ext}(\vec{r}\sigma,\vec{r}\sigma')$. In the local approximation, the exchange-correlation energy density, ε_{xc}, only depends on the diagonal elements, $n\uparrow(\vec{r})$ and $n\downarrow(\vec{r})$, and this so-called local spin density scheme therefore leads to seperate one-electron Schrödinger equations for down- and up-spin electrons. The resulting two band structures must be filled up to a common Fermi level such that the total number of electrons, $n = n\uparrow+n\downarrow$, is the proper one. In this way the spin-up band structure yields the spin-up density, $n\uparrow(\vec{r})$, and the spin-down band structure yields the spin-down density, $n\downarrow(\vec{r})$. The self-consistency condition for the one-electron potential, $v\uparrow(\vec{r})$, experienced by a spin-up electron depends on both the electron, $n(\vec{r}) \equiv n\uparrow(\vec{r}) + n\downarrow(\vec{r})$, and spin-, $m(\vec{r}) = n\uparrow(\vec{r}) - n\downarrow(\vec{r})$, densities. The spin-density enters the exchange-correlation part of the potential only (in the absence of an external magnetic field, spin-orbit coupling etc.) and, to first order in $m(\vec{r})$,

$$v\uparrow(\vec{r}) = v(\vec{r}) - \mu^1_{xc}(n(\vec{r}))\, m(\vec{r}) \tag{63}$$

where the m-independent part of the potential is the one considered in (eqs. 26 and 28). The self-consistency condition for $v\downarrow(\vec{r})$ is (eq. 63) with the minus sign exchanged by a plus.

Using the spin-polarized form of the exchange-correlation potential suggested by von Barth and Hedin (3) and allowing for ferromagnetic (F) polarization we have repeated the self-consistent calculations for the 3d-monoxides as functions of the lattice constant. This requires

twice as many calculations as previously. We find that, for CrO through NiO, within the range of lattice constants considered, the solutions with ferromagnetic polarization are favoured over the solutions without polarization. In none of the cases considered is the spin-polarization, however, complete; this means that the Fermi level always cuts through the spin-up as well as the spin-down metal 3d-band. The values of the spin-polarization, m, obtained for the lattice constant 4.2 Å, are shown in the first column of Table 2. Had the polarization

TABLE 2. Spin-polarized 3d-bandparameters for a = 4.2 A

	n_h	m (μ_B)	$C_{d\downarrow}-C_{d\uparrow}$ (mRy)	I (mRy)	W_d (mRy)	$n_h W_c/5$ (mRy)	$n_h W_d/5\sqrt{2}$ (mRy)
CrO	4	3.35	215	64	415	330	235
MnO	5	4.16	270	65	370	370	260
FeO	4	3.44	220	64	335	270	190
CoO	3	2.40	155	64	305	180	130
NiO	2	0.30	27	-	280	110	80

been complete m would be equal to the number, n_h, of electrons (CrO) or holes (MnO - NiO) in the d-band. In the table we have, furthermore, listed the exchange splittings, $C_{d\downarrow}-C_{d\uparrow}$, of the 3d-bands, the 3d-bandwidths, W_d, and the occupied (CrO) or unoccupied (MnO-NiO) bandwidths $n_h W_d/5$ as naively estimated for a retangular density-of-states shape. In all cases do the latter exceed $C_{d\downarrow}- C_{d\uparrow}$ in accordance with the fact that m is smaller than n_h. The equilibrium lattice constants obtained from the ferromagnetic calculations are shown in Fig. 1 and they are seen not to account fully for the experimental situation. We shall now try to explain these results because,later on, we shall use them in an extrapolation to the antiferromagnetic case.

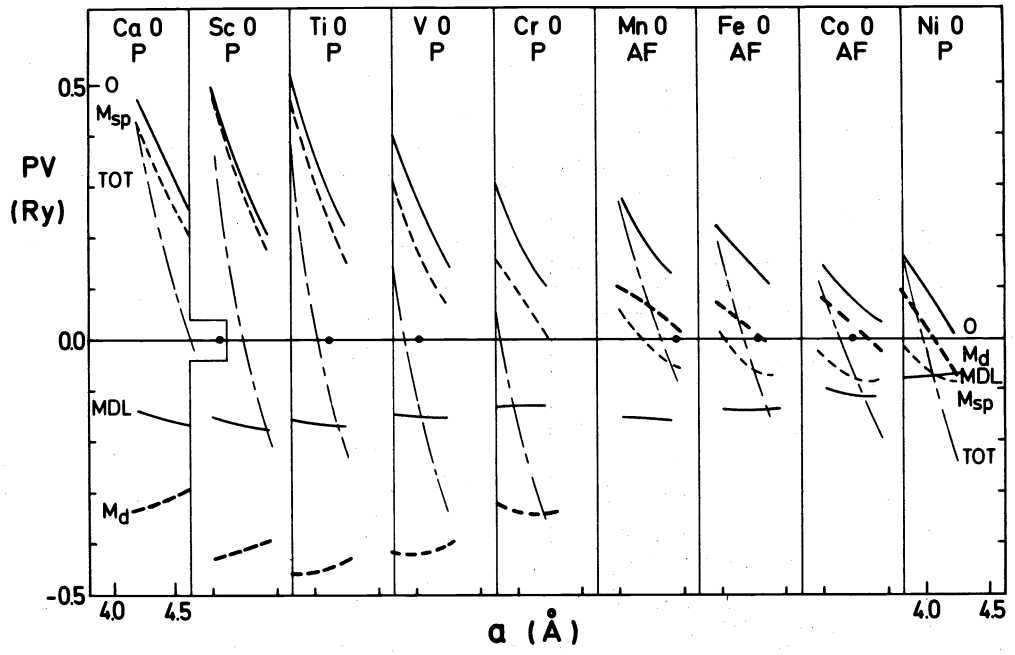

Fig. 16.Partial and total pressures calculated as functions of the lattice constant for the 3d-monoxides in the non-magnetic (P) and antiferromagnetic (AF) phases. The experimental equilibrium lattice constants are indicated by dots and the theoretical lattice constants are where the total pressures vanish. These lattice constants are shown in Fig. 1.

If we use the approximate (eq. 63) for the one-electron potential and further treat the spin-dependent second term by first-order perturbation theory we find that the exchange splitting between the up- and down-spin 3d-band structures is given by

$$\Delta E \equiv E_{d\downarrow}(\vec{k}) - E_{d\uparrow}(\vec{k}) = m\langle\psi_d(\vec{k})|\mu_{xc}^1(n(\vec{r}))m(\vec{r})/m|\psi_d(\vec{k})\rangle$$
$$= m\int^{S_M}\chi_d^2(r)\mu_{xc}^1(n(r))[m(r)/m]r^2dr = mI \qquad (64)$$

Here, the Stoner exchange (-correlation) parameter, I, is only strictly independent of $\vec{k}$ if we assume, as done in the third equation, that the electron- and spin densities are spherically symmetric inside the atomic sphere and if hybridization is neglected. If we divide the exchange splitting, $C_{d\downarrow}-C_{d\uparrow}$, listed in Table 2 with the spin-polarization, m, we obtain the values of I listed in fourth column. Except for NiO, where the numbersinvolved are very small and their ratio therefore uncertain, I appears to be constant through the series. Moreover, we find that I is essentially independent of the lattice constant. For a $\vec{k}$-independent exchange splitting the self-consitency condition for the spin-polarization, m, is that it equals the integral of the (non-polarized) state density, N(E) (per spin), over the range ΔE. A sufficient condition for a ferromagnetic solution is therefore that

$$IN(E_F) > 1 \qquad (65)$$

The density-of-states curves for the monoxides look like the one shown for TiO in Fig. 5, only do the 3d-parts parts scale with W_d as given in Fig. 7. The Fermi level rises as we proceed through the series and, with I^{-1} = 16 states/cell·spin·Ry, we can understand why the ferromagnetic instability is being reached at CrO. The exchange interaction is, however, not strong enough to push the long tail at the bottom of the d-band above the Fermi level for the spin-down electrons and the spin-polarization is therefore not complete. For non-polarized NiO the Fermi level falls above the peak in the state density but, thanks to the small d-bandwidth, the Stoner criterion (eq. 65) is still satisfied although the resulting spin-polarization is small.

In order to explain how ferromagnetic spin-polarization influences the electronic pressure, and in order to prepare ourselves for the antiferromagnetic case, we shall use the simplified pd-model introduced earlier. We first consider the case of MnO where the d-band is half full (f=0.5) and assume that the polarization is complete ($f\uparrow = 1$ and $f\downarrow = 0$). For a half-full band without spin-polarization the dd-bonding pressure (eq. 54) reaches its maximum value

$$[3PV]_{dd\text{-}bond}^{max} = -(25/4)W_d = -2.3 \text{ Ry, for MnO at 4.2 Å,} \qquad (66)$$

and this is completely lost if, instead, we create a full spin-up band and an empty spin-down band. This is the dominating effect of spin-polarization. The pd-covalent bond pressure (eq. 55) is only reduced slightly through the upwards shift of the spin-down d-band by 1/2 mI and the resulting decrease of the pd-hybridization. Specifically:

$$-8N_{pd\downarrow}(C_{d\downarrow}-C_{p\uparrow}) = -4N_{pd}(C_d-C_p)\,[1 + 1/2\ mI\ /\ (C_d-C_p)]^{-1}\ , \qquad (67)$$

as seen from (eq. 19) and neglecting the exchange shift of C_p, which in all cases was found to be an order of magnitude smaller than the exchange shift of C_d. There are similar, small changes caused by the shifts of the d-bands in the metal and oxygen centre pressures. The spin-polarization thus, first of all, influences the pressure by changing the d-band occupancies such that $f\uparrow \neq f\downarrow$ and, secondly, by shifting the d-subbands by the amounts ± 1/2 mI.

Considering now the general case we use the d-band occupation parameters

$$f = (f\uparrow+f\downarrow)/2 \quad \text{and} \quad g = (f\uparrow-f\downarrow)/2 \qquad (68)$$

where, as before, the total number of electrons is $n=N_p+fN_d = 6+10f$ and, in the case of ferromagnetism, the net polarization is $m=gN_d=10g$. The latter does not hold in the case of antiferromagnetism and we shall therefore in the following keep m and g separated. For the dd-bond pressure we obtain from (eq.54)

$$[3PV]_{dd\text{-}bond} = -12.5\ W_d[f\uparrow(1-f\uparrow) + f\downarrow(1-f\downarrow)] = -25\ W_d[f(1-f)-g^2] \qquad (69)$$

The polarization thus causes a repulsion proportional to g^2 which, for the case of complete polarization and a half-full band (f=g=0.5) cancels the first term as seen above. For ferromagnetic MnO our self-consistent calculations (Table 2) gave g=0.416 and therefore a repulsion of 1.6 Ry out of the possible 2.3 Ry. For the pd-bond pressure we obtain from (eq.55), and to first order in $1/2\ mI/(C_d-C_p)$,

$$[3PV]_{pd\text{-}bond} = -4N_{pd\uparrow}(C_{d\uparrow}-C_p)(1-f\uparrow) - 4N_{pd\downarrow}(C_{d\downarrow}-C_p)(1-f\downarrow)$$
$$= -8N_{pd}[(C_d-C_p)(1-f) - 1/2\ mIg] \qquad (70)$$

Here, the polarization gives a small repulsion proportional to mg. According to the discussion following (eq.20) the charge transfer is approximately

$$q=2-N_{pd\uparrow}(1-f\uparrow)-N_{pd\downarrow}(1-f\downarrow)= 2-N_{pd}[(1-f)-mIg/(C_d-C_p)] \quad (71)$$

The charge transfer thus increases proportionally to mg and thereby causes a small attractive Madelung pressure proportional to mg. Finally, it may be realized that, due to the spin-polarization, the metal and oxygen centre contributions have small terms proportional to m^2.

The antiferromagnetic (AF) structure of MnO through NiO is such that the spins on the metal sites in each (111)-plane are aligned and the spins in neighbouring (111)-planes have oposite directions. All the oxygen sites are equivalent and have three metal↑ nearest neighbours and three metal↓ nearest neighbours; consequently, there is no net polarization on the oxygen sites and, in the atomic sphere approximation, the spin-density vanishes in the oxygen spheres. The AF structure has four atoms per primitive cell; two oxygen atoms, a metal↑ and a metal↓ atom. The band structure for a spin-up electron is shown in Fig.17 and consists of six oxygen 2p-bands, five metal↑ 3d-bands, five metal↓ 3d-bands and two hybridized metal↑ - metal↓ 4s-bands. All the bands, of course, hybridize with each others. The band structure for a down-spin electron is identical with the one shown in Fig.17 but, in the assignment of wave functions to the various bands, the metal↑ and metal↓ sites should be interchanged. While the ferromagnetic (F) band-structure problem involves twice as many calculations as the non-magnetic (P) problem, the AF band-structure problem involves matrices of twice the size as those considered previously.This has prevented us from repeating the self-consistent calculations for the AF case and thus to examine the relative stability of the F and AF phases. Instead, we have estimated the equilibrium lattice constants in the AF phase by extrapolation of our findings from the P and F phases.

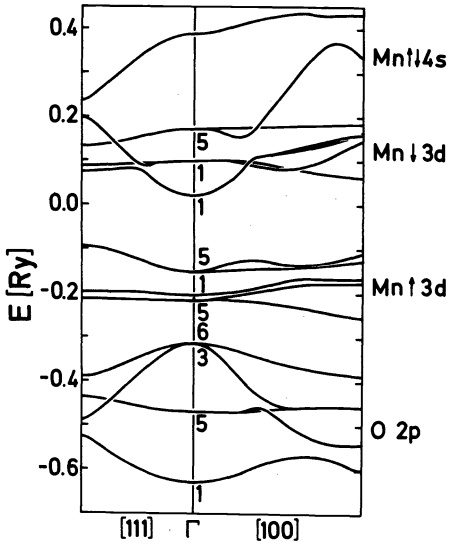

Fig. 17 Antiferromagnetic band-structure for up-spin electrons in MnO as calculated from the self-consistent ferromagnetic atomic-sphere potentials. The [111]-direction is perpendicular to planes of equal spin-direction. a=4.4 Å

Suppose that, for the AF phase, we knew the self-consistent value of thenet spin-polarization in a metal sphere, that is the sublattice magnetization, m. The self-consistent potentials in the spin-up and spin-down metal spheres could then with good accuracy be estimated a extrapolation, linear in m, of the P- and F-potentials obtained self-consistently for the same lattice constant. From our previous calculations the spin-up and spin-down potentials in the oxygen sphere are almost identical and their average is nearly identical to the oxygen potential in the P phase. Also the oxygen potential in the AF phase is therefore well estimated from the extrapolation linear in m of the (average) oxygen potential in the F and P phases. In terms of the pd - model considered above this means that all potential parameters Δ and $(C_\uparrow+C_\downarrow)/2$ are identical in the three phases and only $C_\downarrow - C_\uparrow$ for the metal-sphere orbitals scale linearly with m, i.e. the exchange parameter, I, is the same in the F and AF phases. Now, our aim is to evaluate the elctronic pressure-curves in the AF phase and, for that purpose, the important parameter is the polarization of the d-band occupancies, 5f↑-5f↓=10g, which is to be determined self-consistently with m.If it turns out that the

exchange splitting is so large and the d-subbands so narrow that one d-subband is full or empty, that is, we have strong antiferromagnetism, then it is not so important to determine the exact self-consistent value of m because the crucial parameter, 10g, then attains its maximum value, namely the number of holes in the d-band. This is, for instance, the case for the AF band structure of MnO shown in Fig.17. In MnO the number of electrons in the d-band is 5 and when, as in Fig.17, there is no overlap between the Mn↑ and Mn↓ d-subbands, the lower band will be full and the upper empty such that 10g attains its maximum value of 5. Due to the hybridization between the Mn↑ and Mn↓ bands the sublattice magnetization, m, is not 5, as it would have been for ferromagnetic bands, but smaller. For the case considered in Fig.17 the sublattice magnetization is 4.34 Bohr magnetons and this is made up of the following contributions: The number of up-spin electrons contributed to the Mn↑-sphere is 4.10 from the five Mn↑ 3d-subbands and 1.03 from the six O 2p-subbands. In addition, from the spin-down band structure, the number of down-spin electrons contributed to the Mn↑-sphere is 0.23 from the Mn↓ 3d-subbands and 0.56 from the O 2p-subbands.

As shown in Table 2, the self-consistently obtained magnetizations in the F phase are, except for NiO, less than one Bohr magneton below their maximum possible values, n_h, and, hence, quite close to the value we expect for the AF phase. We have therefore set up band calculations for the AF phase using the atomic-sphere potentials obtained in the ferromagnetic calculations for the same lattice constant and have read off the sublattice magnetization , m, and the d-band polarization, g. For MnO we obtain the result shown in Fig.17 and discussed above. The facts that the d-subbands are well separated and the sublattice mangnetization is self-consistent within 10 per cent is for us a proof that the strongly AF solution is stable, i.e. that

$$10g = n_h \tag{72}$$

The reason why the AF-, in contrast to the F, solutions are strongly polarized is that the AF d-subbands are more narrow than the F d-subbands. As seen from the discussion around (eq.9-13) we realize that the narrowing amounts to nearly a factor $\sqrt{2}$ because the number of Mn↑ atoms neighbouring a given Mn↑ atom is 6 rather than 12. This estimate, which is seen to hold quite well for the full calculation shown in Fig.17, neglects the hybridization between the Mn↑ and Mn↓ d-subbands. The condition for strong antiferromagnetism is essentially that the exchange splitting must exceede $n_h W_d/(5\sqrt{2})$. The latter numbers have been given in the last column of table 2 and they may be compared with the exchange splitting listed in the third column. (It might be remarked that both numbers are too small because of the neglected band-widening and band-repulsion caused by the hybridization between the subbands). Nevertheless the numbers listed do support our belief that the strongly antiferromagnetic solutions are the stable ones for MnO through CoO and that the sublattice magnetizations are not too far from the ferromagnetic magnetizations. In CrO the stable solution seems to be the ferromagnetic one but this has not been experimentally verified because the compound has never been prepared. Our ferromagnetic solution for NiO is weakly magnetic and cannot be used for an axtrapolation to the AF-phase.

The pressure curves estimated for the AF phases of MnO through CoO and shown in Fig.16 have been obtained as follows. Assuming that we can take m over from the ferromagnetic calculations, and that g is given by (eq.72) rather than by 10g=m as in the ferromagnetic case, we simply obtain the AF partial pressures by extrapolation from the corresponding P and F partial pressures: The dd-bond pressure should be scaled by g^2 (eq.69) and then divided by $\sqrt{2}$, the pd-bond and the Madelung pressures should be scaled by g (eqs. 70 and 71), and all the other partial pressures are taken over from the ferromagnetic calculation. Unfortunately our calculations yield the centre- and bond contributions to the p- and d-pressures rather than the dd-bond and pd-bond pressures which are only defined in the simplified model. In this situation we have therefore scaled the p- and d-bond pressures by g^2 and divided the d-bond pressure by $\sqrt{2}$. It turns out that the lattice constants obtained,and shown in Fig. 1, are rather independent of such details. The important contribution is the strong reduction of the metal d-bond pressure caused by the complete filling of one subband and, in the cases of FeO and CoO, the reduction of the remaining contribution by band-narrowing.

This completes the present review of the calculation of electronic structure and ground-state properties using the atomic sphere approximation. As an example we have considered the lattice constants of the 3d transition-metal monoxides. A similar story could be told about the lattice constants shown in Fig.8 of the actinide metals, but not here.

REFERENCES

1. J.C. Slater, Quantum Theory of Molecules and Solids, Vol.4, McGraw-Hill, New York (1974).
2. P. Hohenberg and W. Kohn, Phys. Rev. 136, B864 (1964); W. Kohn and L.J. Sham, Phys.Rev. 140, A1133(1965).
3. L. Hedin and B.I. Lundquist, J.Phys. C4, 2o64 (1971); U. von Barth and L. Hedin, J.Phys. C5, 1629 (1972); O. Gunnarsson and B.I. Lundquist, Phys.Rev. B13, 4274 (1976).
4. J.F. Janak and A.R. Williams, Phys.Rev. B14, 4199 (1976); J.F. Janak, Phys.Rev. B16, 255 (1977).
5. V.L. Moruzzi, A.R. Williams and J.F. Janak, Phys. Rev. B15, 2854 (1977); V.L. Moruzzi, J.F. Janak and A.R. Williams, Calculated Electronic Properties of Metals, Pergamon, New York (1978).
6. O.K. Andersen, J. Madsen, U.K. Poulsen, O. Jepsen and J. Kollar, Physica 86-88B, 249 (1977).
7. D. Glötzel and O.K. Andersen, to be published; results of this work are quoted in Ref.17 below.
8. H.L. Skriver, O.K. Andersen and B. Johansson, Phys.Rev.Lett. 41, 42 (1978).
9. D. Glötzel, J.Phys. F8, L163 (1978).
10. O. Gunnarsson, J. Harris and R.O. Jones, Phys.Rev. B15, 3027 (1977); J.Chem.Phys. 67, 3970 (1977); ibid 68, 1190 (1978); ibid (1979); J. Harris and R.O. Jones, Phys.Rev. A18, 2159 (1978).
11. A.R. Williams, J. Kübler and C.D. Gelatt Jr., Phys.Rev. B (1979); J. Kübler, J.Phys. C8, 2301 (1978); A.R. Williams, C.D. Gelatt Jr. and V.L. Moruzzi in these proceedings.
12. H.L. Skriver, O.K. Andersen and B. Johansson, J.Magnetism and Magnetic Materials, ICM 79 (1980).
13. O.K. Andersen and R.G. Wooley, Mol.Phys. 26, 905 (1973).
14. O.K. Andersen, Phys.Rev. B12, 3060 (1975).
15. O.K. Andersen, Solid State Commun. 13, 133 (1973).
16. O.K. Andersen and O. Jepsen, Physica 91B, 317 (1977).
17. A.R. Mackintosh and O.K. Andersen in Electrons at the Fermi Surface, M. Springford, Ed., Cambridge U.P. (1979).
18. D.G. Pettifor, J.Phys. F7, 613 (1977); ibid F8, 219 (1978).
19. H.L. Skriver, Phys.Rev. B14, 5187 (1976); ibid B15, 1894 (1977); J.P. Jan and H.L. Skriver, J.Phys. F7, 957 (1977); ibid, 1719 (1977); H.L. Skriver and O.K. Andersen, Inst.Phys.Conf. Ser. 39, 100 (1978).
20. G. Arbman and T. Jarlborg, Solid State Commun. 26, 857 (1978); T. Jarlborg, ibid 28, 529 (1978); J.Phys. F9, 283 (1979); ibid, 1065 (1979).
21. D. Glötzel and O.K. Andersen, to be published; T. Jarlborg and A.J. Freeman, to be published.
22. O.K. Andersen, W. Klose and H. Nohl, Phys.Rev. B17, 1209 (1978).
23. A.J. Freeman and T. Jarlborg, J. Appl. Phys. 50, 1876 (1979) and to be published.
24. T. Jarlborg, A.R. Freeman and T.J. Watson-Yang, Phys.Rev.Lett. 39, 1032 (1977).
25. M.S.S. Brooks and D. Glötzel, J.Magnetism and Magnetic Materials, ICM 79 (1980).
26. D. Adler, Solid State Phys. 21,1 (1968).
27. N.F. Mott, Metal-Insulator Transitions, Taylor and Francis, London (1974); and the proceedings.
28. V. Heine and L.F. Mattheiss, J.Phys. C4, L191 (1971).
29. B. Johansson, Phys.Rev. B15, 5890 (1977).
30. For periodic systems a complete identification between Mott insulators and magnetic insulators has been suggested, see B.H. Brandow, Adv.in Physics 26, 651 (1977).
31. T.M. Wilson, Int.J.Quant.Chem.Symp. 3, 757 (1970).
32. L.F. Mattheiss, Phys.Rev. B5, 290 (1972); ibid, 306 (1972).
33. A. Neckel, P. Rastl, R. Eibler, P. Weinberger and K. Schwarz, J.Phys. C9, 579 (1976); Ber. Bunsen-Ges. Phys.Chem. 79, 1053 (1975).
34. K. Schwarz, J.Phys. C10, 195 (1977); K. Schwarz and A. Nechel, Phys.Rev. B19, 5439 (1979).

35. J. Korringa, Physica 13, 392 (1947); W. Kohn and J. Rostocker, Phys.Rev. 94, 1111 (1954).
36. K.H. Johnson, J.Chem.Phys. 45, 3085 (1966).
37. J.C. Slater and G.F. Koster, Phys.Rev. 94, 1498 (1954).